

Article

Better Ce (III) Sorption Properties of Unprocessed Chitinous Waste from *Hermetia illucens* than Commercial Chitosans

Justyna Bąk ¹, Piotr Bulak ^{2,*}, Monika Kaczor ², Dorota Kołodyńska ¹ and Andrzej Bieganski ²

¹ Department of Inorganic Chemistry, Institute of Chemical Sciences, Faculty of Chemistry, Maria Curie-Skłodowska University, Maria Curie-Skłodowska Sq. 2, 20-031 Lublin, Poland; justyna.bak@mail.umcs.pl (J.B.); dorota.kolodynska@mail.umcs.pl (D.K.)

² Institute of Agrophysics, Polish Academy of Sciences, Doświadczalna 4, 20-290 Lublin, Poland; m.kaczor@ipan.lublin.pl (M.K.); a.bieganski@ipan.lublin.pl (A.B.)

* Correspondence: p.bulak@ipan.lublin.pl

Abstract: Insect farming generates a new type of chitinous waste in the form of dead specimens that have died of natural causes and insect moults (puparia), particularly large amounts of which are generated during the rearing of holometabolous insects. Following the circular economy paradigm, we treated waste in the form of puparia and dead adults of *H. illucens* as a valuable material, i.e., as sources of chitin, and tested it as a sorbent for cerium, a lanthanide of great industrial importance. For comparison, non-treated, raw insect materials and commercial chitosans were also investigated. Chitin extracted from *H. illucens* showed an adsorption capacity at the same level as commercially available, marine-source chitin (approximately 6 mg Ce·g⁻¹). However, more interestingly, raw materials exhibited much higher adsorption capacities—dead adults were similar to commercial chitosans (approximately 32 mg Ce·g⁻¹), while puparia demonstrated twice the performance (approximately 60 mg Ce·g⁻¹). This indicates that unprocessed waste can be used as environmentally friendly, cost-effective Ce biosorbents with comparable or even better sorption capacity than chitosans, whose production requires intense chemical processing.

Keywords: black soldier fly; chitin; waste biomass; cerium; biosorbent; rare earth elements; *Hermetia illucens*; waste



Citation: Bąk, J.; Bulak, P.; Kaczor, M.; Kołodyńska, D.; Bieganski, A. Better Ce (III) Sorption Properties of Unprocessed Chitinous Waste from *Hermetia illucens* than Commercial Chitosans. *Materials* **2024**, *17*, 5255. <https://doi.org/10.3390/ma17215255>

Academic Editor: Antonio Gil Bravo

Received: 25 September 2024

Revised: 22 October 2024

Accepted: 25 October 2024

Published: 29 October 2024



Copyright: © 2024 by the authors. Licensee MDPI, Basel, Switzerland. This article is an open access article distributed under the terms and conditions of the Creative Commons Attribution (CC BY) license (<https://creativecommons.org/licenses/by/4.0/>).

1. Introduction

Rare earth elements (REE) are represented by all the elements of the lanthanide group, as well as scandium and yttrium [1]. These elements are characterized by having similar physical and chemical properties, and their potential in technological applications depends on their unique catalytic [2], magnetic [3] and optical [4] properties. Their use in various technological processes is highly indispensable. REE are applicable in areas such as electronics and various medical fields, as well as manufacturing, technology, and renewable energy [5].

One of the most mentioned lanthanides is cerium. Its abundance in the earth's crust is approximately 63 mg·kg⁻¹ [6]. In industrial applications, it is most commonly used as a catalyst, e.g., in chemical processes, automotive technologies or petroleum refining, in polishing techniques, or as a luminophore in electronic devices [7]. However, it is also utilized in biomedical applications in the form of antimicrobial nanocompounds [8], and it may have potential usage in hydrogen production [9].

The consequence of the wide use of cerium in industry is the need to recover it at the end of the life cycle of the products in which it is found. This is important for both environmental and economic reasons. The extraction of cerium, whether from ore or through its recovery from end-of-life products containing it, mainly involves the phenomenon of sorption. This is because this procedure can be highly selective and can also process low-concentration sources. A broad variety of substances, including biosorbents, carbon-based

supports and inorganic sorbents, as well as chelating and ionic-exchange resins, have been evaluated for their use in the sorption of cerium and REE [10].

Biosorbents are particularly interesting materials because they usually do not require pre-processing, or when they do it is quite simple to carry out. The basis of biosorption depends on the ability to bind various compounds (e.g., metals) on the surface of a given material (biosorbent) [11]. In the case of Ce sorption, there are a number of studies on different types of biosorbents. Among them, we can find methacrylic acid-grafted chitin with a sorption capacity of 147 mg Ce/g [12], marine chitosan and its analogues (29.45–119.48 mg Ce/g) [13], thiosalicylic-modified/ion-imprinted chitosan (164 mg Ce/g) [14], active carbons modified by KMnO₄ (48–71 mg Ce/g) [15]. The given examples of biosorbents, despite their high sorption capacity, require operating costs and are not neutral to the environment due to the use of various chemicals for their production. More environmentally friendly examples of biosorbents include plant-based biosorbents, e.g., *Platanus orientalis* leaf powder, which showed a sorption capacity of 32.05 mg/g Ce [16], bacterial biomass of *Spirulina* (38.2 mg Ce/g) [17], and algal biosorbents of *Turbinaria conoides* (152.9 mg Ce/g) [18]. In the case of these examples, sorption occurred on unprocessed materials, but their biomass was still produced specifically for these purposes. This indicates the need to find biomaterials with already high sorption properties for, e.g., the removal of heavy metals or precious elements, such as REE. The search for biosorbents with a high capacity for Ce should align with the circular economy paradigm, which is based on the utilization of waste materials from one industrial branch as a source substrate for others, or its direct usage in new contexts. An example of such an approach can be the use of waste in the form of crab shell particles, which had a sorption capacity of 144.9 mg Ce/g, but this material needed acid pretreatment to remove excess calcium carbonate contained in it [19]. The less processed/modified the biosorbent is, the better it is in terms of costs and environmental aspects (no energy inputs and no consumption of chemical reagents).

In recent years, the market for the production of insects has been developing quite intensively. Their relatively simple breeding process allows for obtaining a high-protein product used in the feed industry [20]. One example of such insects is *Hermetia illucens*, which belongs to the family Stratiomyidae from the Diptera order [21]. This fly represents one of the holometabolous insects, which are characterized by a developmental cycle that passes through the pupa stage. This is followed by the adult form (imago), which leaves puparia (empty pupae molts) after hatching [22]. This kind of insect waste has various applications, including as a substrate for biochar production [23] or material for insect chitin extraction [24]. Increased interest in insect production will result in larger amounts of post-breeding residues as well as chitinous insect wastes, like puparia or dead adults after the end of their life cycle, which should be managed while taking into account the environmental policy of a circular economy.

Therefore, the main aim of this research was to examine the sorption properties of *H. illucens* post-breeding remains (in the form of the puparia and dead adults of the insect) in relation to cerium ions. We hypothesized that such unprocessed material would be a good cerium sorbent. However, due to the fact that chitin sorbents obtained from other organisms are available on the market, an additional aim of this work was to check the sorption capabilities of pure chitin isolated from breeding pristine wastes—also from puparia and dead adults of the insect. The hypothesis underlying the implementation of the additional aim was the assumption that cerium sorption on chitin from *H. illucens* would be at least as effective as on commercially available chitin from marine origins.

2. Materials and Methods

2.1. Insect Breeding

H. illucens larvae were reared in the laboratory of the Institute of Agrophysics of the Polish Academy of Sciences in Lublin (Poland). The larvae were fed with commercial carp fish feed (FloraZoo, Chełmża, Poland) with the following composition (values given per dry weight): 54.80% carbohydrates, 25.00% protein, 5.00% fat and oil, 5.80% crude fiber,

5.70% ash, 1.25% lysine, 1.00% calcium, 0.97% phosphorus and 0.40% methionine. The culture temperature was 27 ± 1 °C with a substrate humidity of 50%–80% [25]. The insects were kept in darkness until the pupae occurred after 16 days. They were then collected and transferred to the breeding container where the adults emerged (photoperiod 12/12, air relative humidity 60%, 25 ± 1 °C). The empty puparia were collected for further processing at this stage. Under these conditions, the adult flies reproduced and lived for up to five days. During this time, they were provided with access to water. After mating, the adults died of natural causes and were removed from the chamber.

2.2. Chitin Extraction

Sodium hydroxide, hydrochloric acid, ethanol and hydrogen peroxide (30%) were acquired from Standard (Lublin, Poland). The empty puparia and dead flies were cleaned utilizing ethanol and water, then dried at 60 °C for 24 h and ground. Size distribution can be found in Table S1 (in the Supplementary Materials). Chitin extraction was then performed (Figure 1) according to Złotko et al. [26].

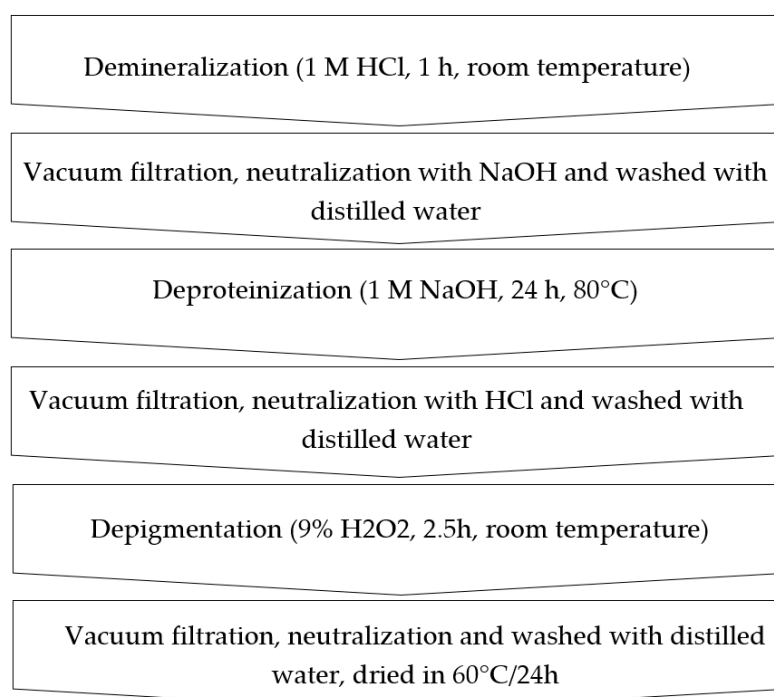


Figure 1. Scheme of chitin extraction from *H. illucens* puparia and dead flies.

2.3. Sorbents

The following materials have been used for the experiments assessing the adsorption of Ce(III) ions: commercial chitin, chitin obtained from *H. illucens* adults (flies)—Ch-A, chitin derived from *H. illucens* puparia—Ch-P, the ground form of *H. illucens* adults—A, the ground form of *H. illucens* puparia—P, high-molecular-weight commercial chitosan—CS-HW, medium-molecular-weight commercial chitosan—CS-MW, and low-molecular-weight commercial chitosan—CS-LW.

Commercial chitin derived from shrimp shells was purchased from Sigma Aldrich (Burlington, MA, USA) (chemical formula: $(C_8H_{13}NO_5)_n$, powder form). In addition, chitosan samples of different molecular weights (CS-HW, CS-MW and CS-LW) acquired from Sigma Aldrich (Burlington, MA, USA) were used to compare the efficiency of the removal of cerium(III) ions from aqueous solutions. All types of chitosan have the chemical formula $C_{12}H_{24}ClN_2O_9$ and occur in a powder form.

Prior to analysis, samples of Ch-A, Ch-P, A and P were ground with an IKA laboratory mill (Tube Mill Control, DanLab, Białystok, Poland). The characterization of the particle

distribution of the obtained powders was carried out with an automated particle classification system, Morphology G3 (Malvern Panalytical, Malvern, Great Britain). Particle size distributions are given in Table S1.

2.4. Physicochemical Characterization

The materials underwent X-ray diffraction (XRD) characterization and infrared spectroscopy attenuated total reflectance Fourier-transform infrared (ATR-FTIR) analysis was conducted before the sorption process. Measurements of N₂ adsorption/desorption isotherms were carried out using the accelerated surface area and porosimetry system (ASAP) method before sorption. Subsequently, scanning electron microscopy (SEM), coupled with energy-dispersive X-ray spectroscopy (EDX), was employed to examine the materials after the sorption process.

For the X-ray diffraction analysis, the mineral composition was determined using the powder method with the Panalytical X'Pert PROMPD X-ray diffractometer, which featured the PW 3050/60 goniometer and operated in the 2 θ angle range of 5–65 degrees (Malvern Panalytical, Malvern, Great Britain). The X-ray source utilized was a copper lamp (CuK = 0.154178 nm). The ground, well-distributed sample was placed in a special XRD holder, which is made of a material that does not reflect X-rays. The basis of the XRD method is the phenomenon of X-ray diffraction on the crystal lattice of a substance. Data analysis was performed with the X'Pert High Score software.

In the case of ATR-FTIR spectroscopy, the spectra of the eight sorbents were recorded before the sorption using the ATR technique. This analysis was conducted within the wavelength range of 550–4000 cm⁻¹, employing the Agilent Cary 630 FTIR spectrometer (Agilent Technologies, Santa Clara, CA, USA). ATR-FTIR spectra were performed by placing a sample of about 0.2 g directly on a diamond crystal and pressing the sample against the crystal to ensure adequate contact. The spectroscope then collects the data without further sample processing. Spectral data were recorded with the Micro Lab PC program, and a subsequent evaluation of the spectra was carried out with the Agilent Resolutions Pro software (Agilent Technologies, Santa Clara, CA, USA).

An ASAP 2420M (Micromeritics Instrument Corporation, Norcross, GA, USA) sorption analyzer was used to calculate the low-temperature N₂ adsorption/desorption isotherms. The materials (0.1 g) were degassed at 105 °C in a glass tube before the measurements were taken for removing volatile components of the samples. Both the surface area and the pore size distribution were calculated with the Barrett-Joyner-Halenda (BJH) and Brunauer-Emmett-Teller (BET) methods, respectively.

The Quanta 250 FEG scanning electron microscope (SEM) (FEI, Hillsboro, OR, USA) equipped with energy-dispersive X-ray spectroscopy (EDX) was used to study the microstructural morphology and elemental composition following the sorption process. Before the surface morphology was measured, a sample was placed on a special pad, sputtered with a carbon-conductive material, and then placed in the chamber of the microscope.

2.5. Batch Sorption Test

To evaluate the effectiveness of the sorption process, batch sorption tests were conducted involving the removal of Ce(III) ions using eight biopolymers from water media. As a source of cerium(III) ions, cerium nitrate hexahydrate (Avantor Performance Materials, Gliwice, Poland) was utilized at a concentration of 1000 mg·L⁻¹. First, the effect of the solution pH (2.0–6.0) on the sorption process was tested by weighing 0.04 g of sorbents (commercial chitin, CS-HW, CS-MW, CS-LW) and shaking in a solution of cerium(III) ions (20 mL) with an initial concentration of 50 mg·L⁻¹ for 300 min. Studies of the optimal pH selection (pHM82, Radiometer, Copenhagen, Denmark) were performed for the commercial biopolymers due to the limited amount of remains. Then, after applying the same starting concentration of 50 mg·L⁻¹, the kinetic investigation was carried out at various adsorption times (0–300 min). In addition, evaluations of the effect of the initial concentra-

tion ($10\text{--}200\text{ mg}\cdot\text{L}^{-1}$) on the sorption process (isotherm studies) were also performed at a constant shaking time of 300 min.

In summary, shaking was carried out at various times (0–300 min) and initial concentrations ($10\text{--}200\text{ mg}\cdot\text{L}^{-1}$) at a pH of 3.0 (optimum pH) and a temperature of $25\text{ }^{\circ}\text{C}$, at a rate of 180 rpm. A laboratory shaker (type 458A, Elpin Plus, Lubawa, Poland) was used for static tests. Nitric acid and/or sodium hydroxide (Chempur, Piekary Śląskie, Poland) solutions in small amounts were added to adjust the pH, which was measured by a pHM82 pH meter (Radiometer, Copenhagen, Denmark). Each time, the suspension was immediately filtered after the specified time period and the concentration of cerium(III) ions was detected by inductively coupled plasma optical emission spectroscopy (ICP-OES, type 720, Varian, Palo Alto, CA, USA). The concentration of Ce(III) ions was determined with the following parameters: wavelength of 446.021 nm, resolution of 0.004 nm, reading time of 10 s, sampling delay of 15 s, pump speed of 15 s and rinse time in the range of 12–15 s. Filtration was performed using quantitative-medium sieves to separate the sorbent from the solution, which made it possible to determine the concentration of Ce(III) ions in the solution after the sorption process. Errors were noted during the triplicate testing and are represented in the figures as 5% error margins.

2.6. Analytical Methods

This subsection presents (in the Supplementary Materials) the formulas used to calculate the amounts of adsorbed ions, equilibrium capacities, and nonlinear forms of the kinetic and isotherm models, as well as the correlation coefficient and Chi-square error.

3. Results and Discussion

3.1. The Change in the Physicochemical Properties of Biopolymers

3.1.1. Mineral Composition

The mineral composition of the eight sorbents, as determined by X-ray diffraction (XRD), is shown in Figure 2.

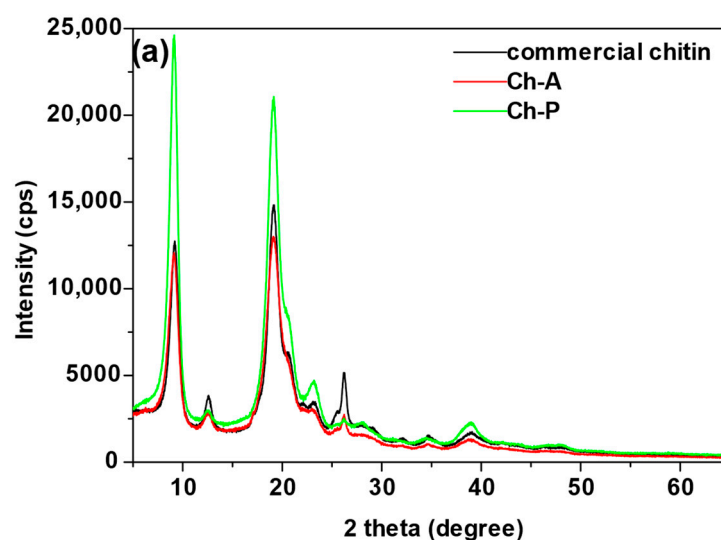


Figure 2. Cont.

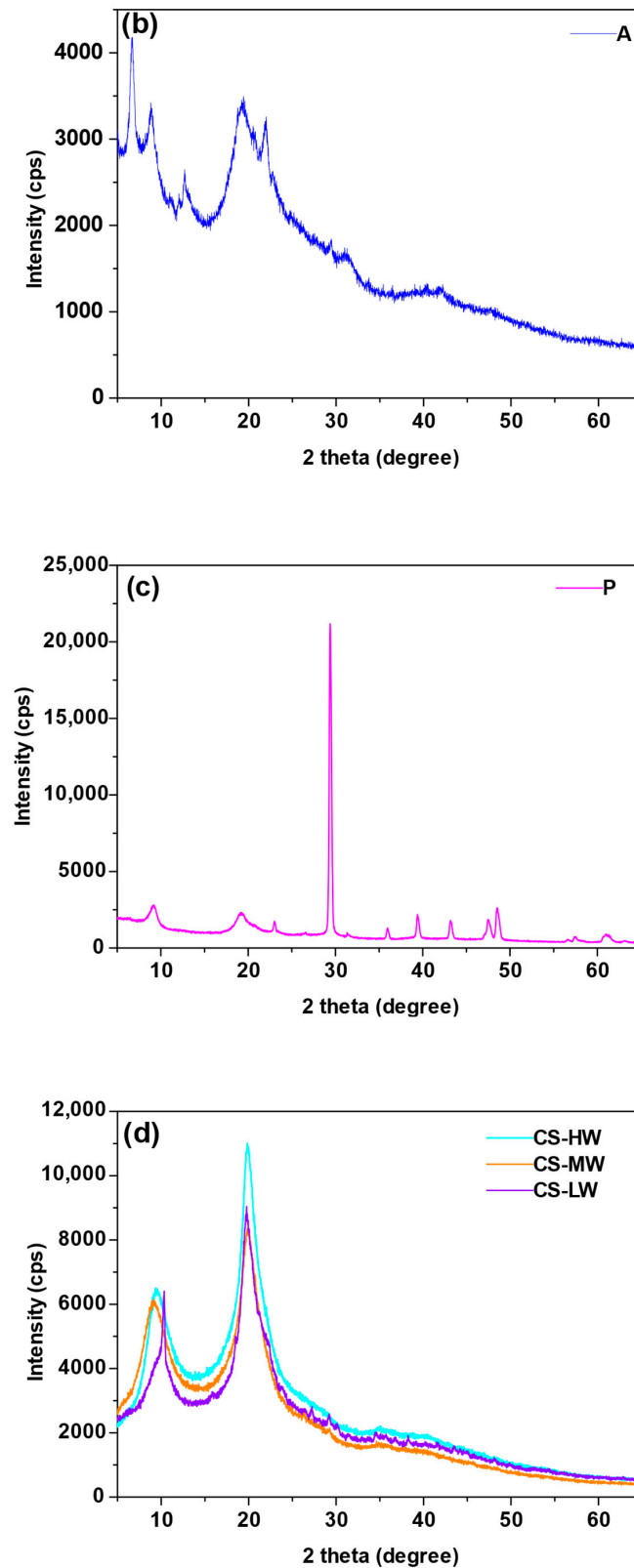


Figure 2. X-ray diffractometry analysis of (a) commercial chitin, chitin obtained from *H. illucens* adults (Ch-A), chitin derived from *H. illucens* puparia (Ch-P), (b) the ground form of *H. illucens* adults (A), (c) the ground form of *H. illucens* puparia (P), (d) high-molecular-weight commercial chitosan (CS-HW), medium-molecular-weight commercial chitosan (CS-MW), and low-molecular-weight commercial chitosan (CS-LW).

In the case of commercial chitin, the primary peak occurs at $2\theta = 19.2$. This is a diffraction peak corresponding to the N-glucosamine in the chain, while the secondary peak at $2\theta = 9.1$ is smaller and is due to the presence of N-acetyl-D-glucosamine [27]. The existence of these peaks indicates the crystalline structure of chitin, which can occur in three forms: α , β or γ [28]. Additional peaks at 2θ angles of 26.2 and 38.9 are characteristic of silica. The similarity of the spectra of chitin samples (Ch-A and Ch-P) to the XRD spectrum of commercial chitin testifies to the efficiency of chitin synthesis based on these waste materials. In the case of Ch-A and Ch-P, there are two characteristic diffraction peaks in the spectrum with the highest intensities at 2θ angles of 9.1 and 19.1. These results agree with those obtained by Waśko et al. [29], who characterized chitin obtained from the puparium of *H. illucens* and determined its α form of crystallinity. Other peaks with low intensities at 2θ angles 26.2, 34.6 and 38.9 are characteristic of silica.

In the case of the spectrum of the sample derived from grinding the adults (A), a number of peaks appear, and two of them at 2θ angles 22.0 and 31.9 are matched by calcium and aluminum silicate. This spectrum shows a raised background, indicating the presence of amorphous substances in this sample. As for the spectrum of the sample attained by grinding *H. illucens* fly puparia (P), peaks matching calcium carbonate were obtained at the following 2θ angles: 23.0, 29.3, 35.9, 39.4, 43.3, 47.5 and 48.5. For all the chitosan samples (CS-HW, CS-MW, CS-LW), two characteristic broad peaks are observed in the X-ray diffraction spectrum. The primary peak of chitosan corresponds to $-\text{NH}_2$ groups in amine II and occurs at 2θ equal to 19.9. At 2θ equal to 9.4 there is a secondary peak. This is a less intense diffraction peak, which is related to the existence of $-\text{N}-\text{CO}-\text{CH}_3$ groups in amine I contained in the structure of chitosan [30].

3.1.2. The Presence of Functional Groups

Based on ATR-FTIR analysis (Figure 3), it is possible to indicate the characteristic surface functional groups of the materials. For all the sorbents, the peaks in the range of $3800\text{--}3400\text{ cm}^{-1}$ and $3350\text{--}3200\text{ cm}^{-1}$ correspond to O-H and N-H bonding stretching vibrations, respectively [31,32]. In the case of sorbent A, these peaks have the lowest intensities. High-intensity peaks at approximately $2920\text{--}2850\text{ cm}^{-1}$ are considered responsible for the C-H stretching vibration in aliphatic chains [33]. In some cases, such as in the Ch-P and A samples, there are two peaks associated with these vibrations. The existence of a peak at approximately 1640 cm^{-1} (stretching of C=O groups in amide groups, amide I band) has been used to confirm the presence of residual N-acetyl groups. The amide II band (1550 cm^{-1}) corresponds to the bending vibrations of N-H groups in amide [34–36].

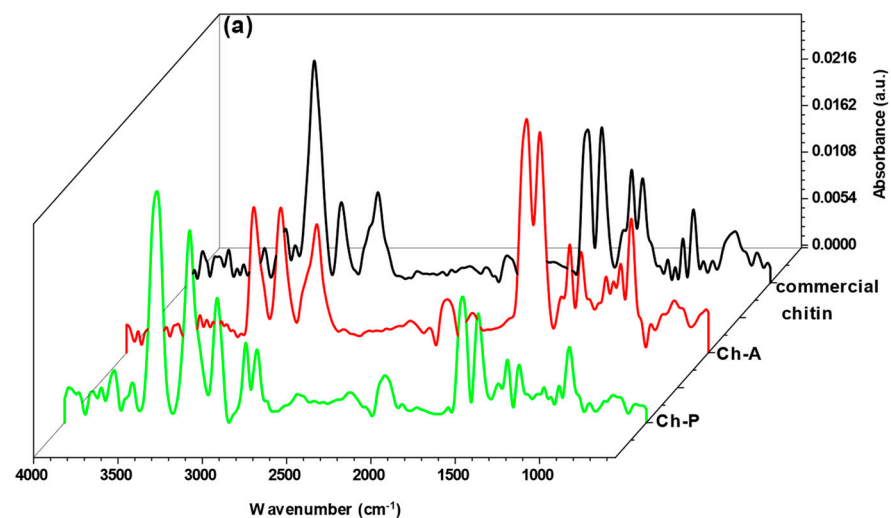


Figure 3. Cont.

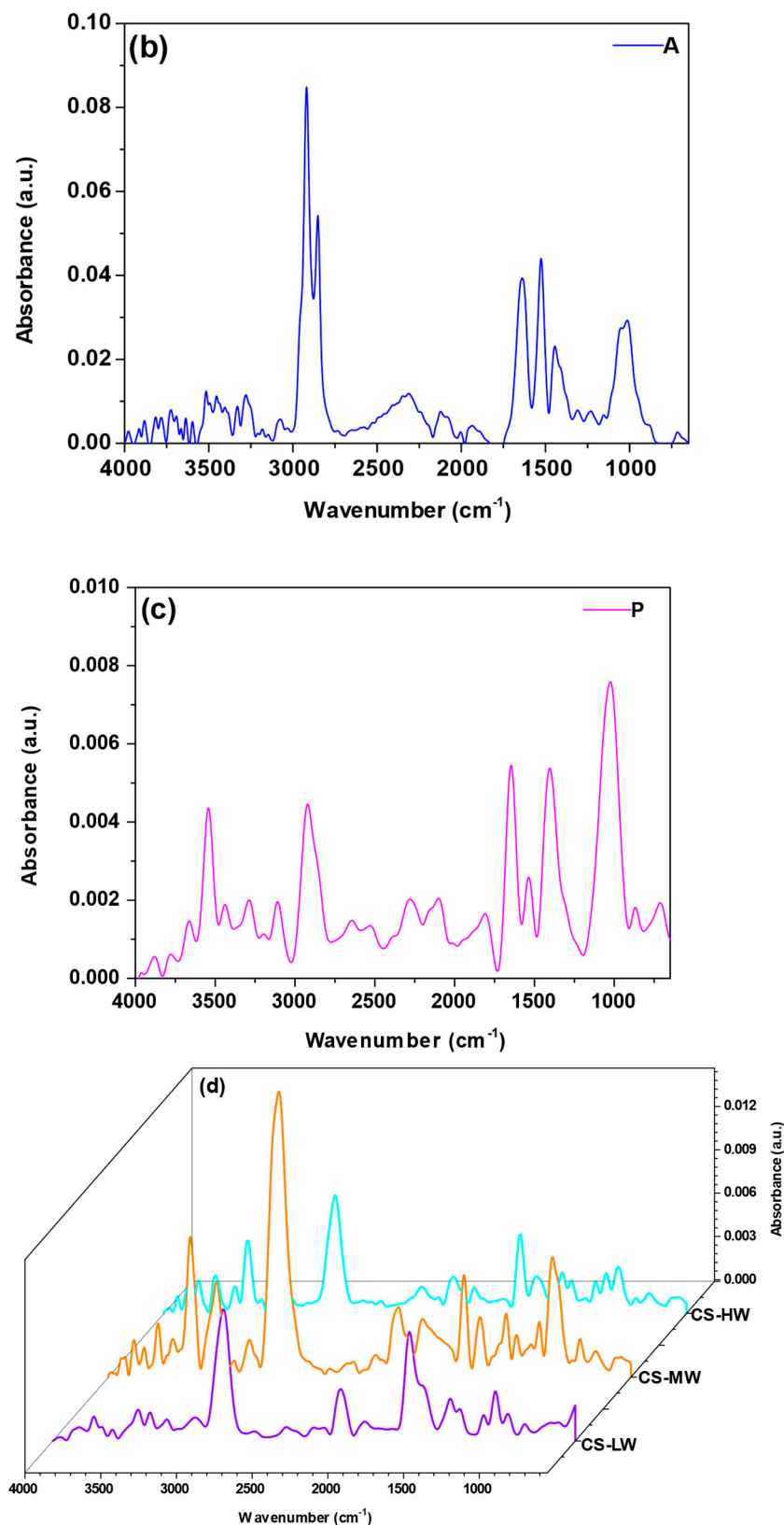


Figure 3. ATR-FTIR method of (a) commercial chitin, chitin obtained from *H. illucens* adults (Ch-A), chitin derived from *H. illucens* puparia (Ch-P), (b) the ground form of *H. illucens* adults (A), (c) the ground form of *H. illucens* puparia (P), (d) high-molecular-weight commercial chitosan (CS-HW), medium-molecular-weight commercial chitosan (CS-MW), and low-molecular-weight commercial chitosan (CS-LW).

In the case of the chitosans (CS-HW, CS-MW, CS-LW), the intensity of the peaks at 1640 and 1550 cm^{-1} is lower than that of the commercial chitin, Ch-A and Ch-P samples. This difference can be attributed to the deacetylation reaction, during which some of the acetamide groups of chitin are converted to amino groups [37,38]. In the A, P and CS-HW samples, the peaks appear at approximately 1420 cm^{-1} , originating from the bending vibrations of CH_2 groups. In some sorbents, including the commercial chitin, Ch-A, Ch-P, CS-HW, CS-MW and CS-LW samples, peaks emerge at approximately 1370 cm^{-1} , linked to the presence of deformation vibrations from CH_3 groups. With the exception of sample P, the amide III band (1310 cm^{-1}) indicates the existence of C-N groups in the sorbents [34,35]. These peaks are characterized by less intense absorbance. In addition, C-O-C vibrations are associated with the band between 1070 and 1000 cm^{-1} [39,40]. The occurrence of C-N and C-C groups is further evidenced by small peaks that become visible at approximately 870 cm^{-1} [41].

3.1.3. Porosity Characteristics

Based on the gas porosimetry method, the specific surface area, pore diameter and pore volume of the eight materials have been determined. The results are shown in Table 1.

Table 1. Physical characteristics of commercial chitin, chitin obtained from *H. illucens* adults (Ch-A), chitin derived from *H. illucens* puparia (Ch-P), the ground form of *H. illucens* adults (A), the ground form of *H. illucens* puparia (P), high-molecular-weight commercial chitosan (CS-HW), medium-molecular-weight commercial chitosan (CS-MW), and low-molecular-weight commercial chitosan (CS-LW).

Materials	BET Surface Area ($\text{m}^2 \cdot \text{g}^{-1}$)	Average Pore Diameter (nm)	Pore Volume ($\text{cm}^3 \cdot \text{g}^{-1}$)
Commercial chitin	5.28	15.8	0.0238
Ch-A	2.15	7.7	0.0068
Ch-P	0.11	22.7	0.0043
A	1.46	12.1	0.0053
P	0.03	41.4	0.0039
CS-HW	0.32	32.8	0.0017
CS-MW	1.21	11.9	0.0038
CS-LW	0.60	34.9	0.0036

The gas adsorption porosimetry results reveal significant variations in the surface area and pore size distribution of the tested biopolymers. Commercial chitin exhibits the highest specific surface area at 5.28 $\text{m}^2 \cdot \text{g}^{-1}$, indicating that there is a relatively high surface area available for adsorption processes. In contrast, Ch-P and P have the lowest specific surface areas of 0.11 $\text{m}^2 \cdot \text{g}^{-1}$ and 0.03 $\text{m}^2 \cdot \text{g}^{-1}$, respectively, suggesting that they have fewer exposed surface areas for adsorption. Of the chitosan groups, CS-MW has the largest specific surface area of 1.21 $\text{m}^2 \cdot \text{g}^{-1}$. Regarding the pore diameter, P has the largest pores, with an average diameter of 41.4 nm, followed by CS-LW with a pore diameter of 34.9 nm. Ch-A has the smallest pores, with an average diameter of 7.7 nm. From these data, it is possible to determine which pore sizes dominate in each material. Mesopores and even macropores are dominant in sample P. In addition, a predominance of mesopores is found in the samples of commercial chitin, Ch-P, A, CS-HW, CS-MW and CS-LW. In contrast, mesopores and micropores are present in the Ch-A sample. Pore diameter is an essential parameter as it can influence the types of molecules that can be adsorbed. In addition, the pore volume was also determined. Among the tested commercial sorbents, the highest pore volume was obtained for chitin 0.0238 $\text{cm}^3 \cdot \text{g}^{-1}$. From the group of Ch-A, Ch-P, A and P sorbents, the largest pore volume was obtained for Ch-A 0.0068 $\text{cm}^3 \cdot \text{g}^{-1}$.

3.1.4. Morphology and Elemental Composition

SEM analysis shows the surface shape of the isolated chitin particles as well as the starting materials (Figure 4a–d). The surface of the chitins is much smoother than that of raw

adults and puparia. The chitin from adults is particularly smooth, and in the foreground, the exoskeleton covering the insect’s compound eye can likely be observed. Individual cavities in this fragment correspond to the single ommatidia. Chitin from puparia (Ch-P) has a surface composed of superimposed plates dotted with numerous pits.

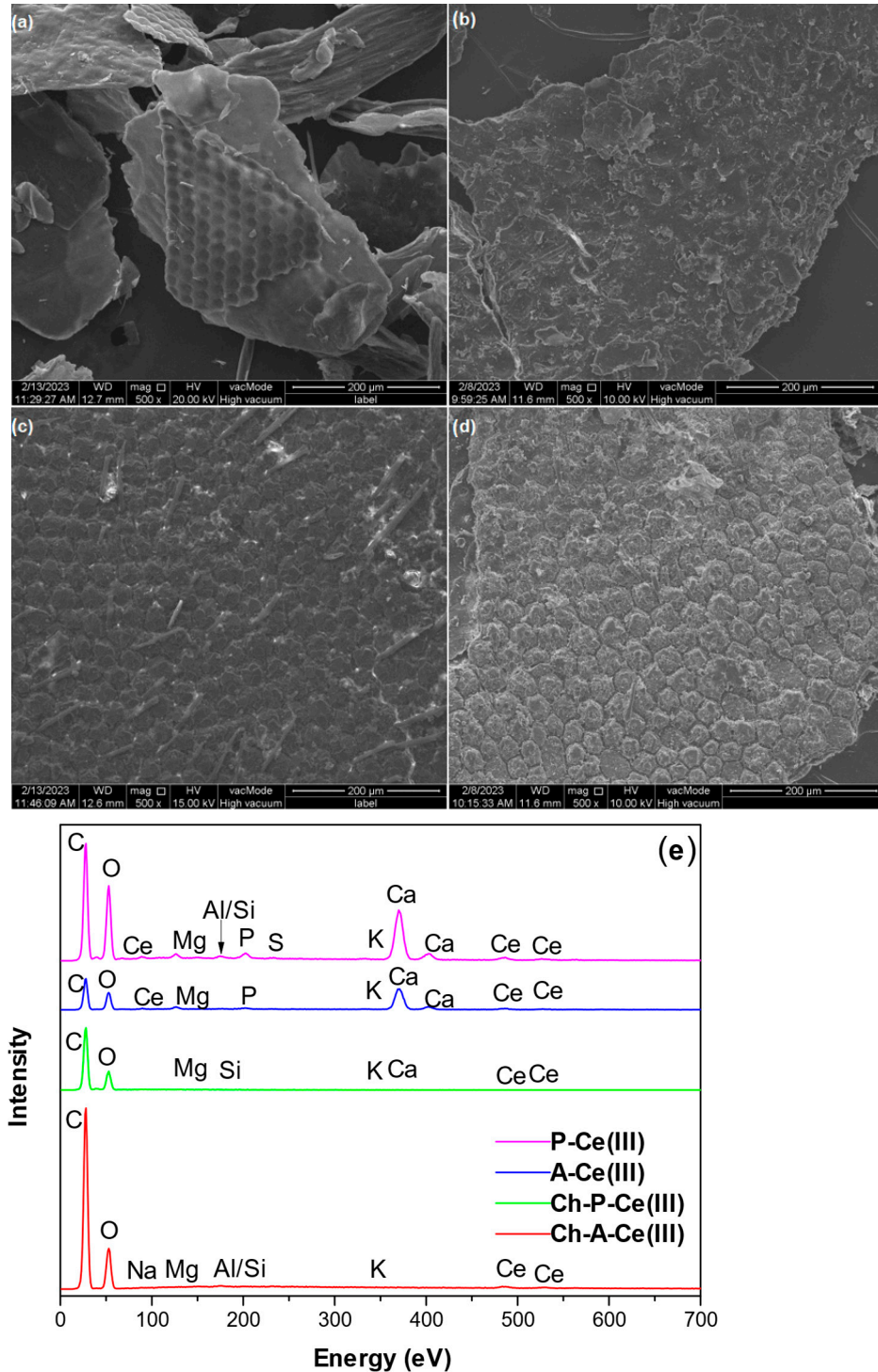


Figure 4. Morphology of the samples under 500x magnification in SEM: (a) chitin obtained from *H. illucens* adults (Ch-A), (b) chitin derived from *H. illucens* puparia (Ch-P), (c) the ground form of *H. illucens* adults (A), (d) the ground form of *H. illucens* puparia (P), (e) EDS patterns for Ch-A, Ch-P, A, P after Ce sorption.

The ground exoskeletons of adults and puparia exhibit a clearly visible structure approximately resembling a honeycomb. The description of this type of surface also appears in other publications characterizing the microstructure of *H. illucens* [23,24,42]. In the case of the adults, numerous sensory hairs are visible, while the puparium surface in the captured fragment contains a much smaller number of them.

Samples of investigated materials after Ce(III) adsorption were also analyzed through energy-dispersive spectroscopy (Figure 4e). EDS spectra for commercial chitin and chitosans are presented in Figure S1 (in the Supplementary Materials). All the materials show the presence of Ce. In the samples of Ch-A and Ch-P, the occurrence of Si can be connected to silica identified by XRD in both of the samples. In A and P, a peak for Ca is clearly visible, which is not seen in the Ch-P and Ch-A samples, and which can be linked to the incidence of CaCO_3 in the *H. illucens* exoskeleton [43]. This compound has also been detected by XRD analysis in the P sample. The occurrence of CaCO_3 may influence the higher sorption capacity of Ce (III) ions by A and P compared to their chitin isolates. The presence of this compound may lead to carbonate ions-mediated microprecipitation process and subsequent deposition on the “rough” surface of these materials (Figure 3a,b) [19]. Other elements like Mg, Al, Na, Si, P, S, and K, detected in minor quantities in the samples, occur naturally in *H. illucens* in significant quantities [44]. In research publications it can be found that demineralization of the sample during chitin extraction is never complete, which is why the EDS spectra for Ch-P and Ch-A also contain mineral peak (Figure 3). For example, Hahn et al. [45] also using hydrochloric acid obtained mineral removal of approximately 90% for puparia. For other types of reagents, e.g., formic acid, demineralization of 85% was achieved for puparia and 87% for flies [46]. However, higher efficiencies can be obtained with natural deep eutectic solvents of approximately 98% [47].

3.2. Cerium(III) Ions Sorption Characteristics

3.2.1. pH Test

In general, pH is regarded as a significant factor that regulates the processes of adsorption at water-adsorbent interfaces. The impact of the initial solution pH (Figure 5) was investigated in order to establish the ideal conditions for the cerium(III) ions sorption on biopolymers. Due to the limited number of Ch-A, Ch-P, A and P samples, studies of the effect of pH were conducted only on commercially purchased materials.

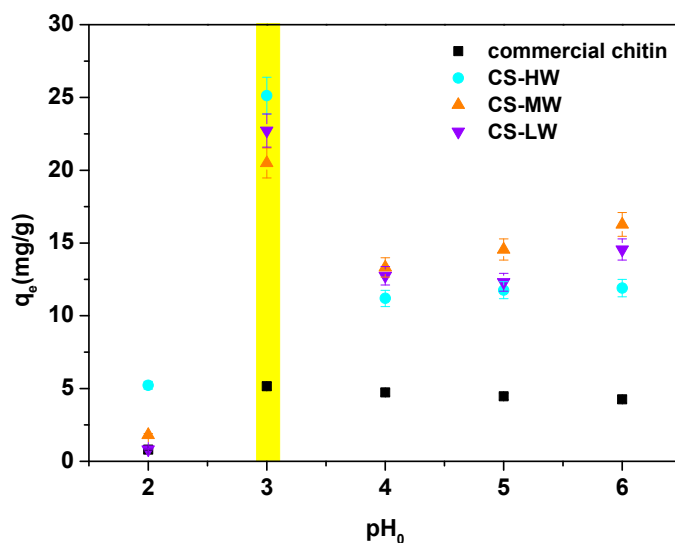


Figure 5. pH effect for the Ce(III) ions sorption on commercial chitin, high-molecular-weight commercial chitosan (CS-HW), medium-molecular-weight commercial chitosan (CS-MW), and low-molecular-weight commercial chitosan (CS-LW) (C_0 50 $\text{mg}\cdot\text{L}^{-1}$, t 300 min., T 25 °C, 180 rpm). Yellow line indicated the most interesting result.

Figure 5 shows that the sorption efficiency has a strong dependence on the solution pH. The optimum is found at a pH of 3.0 and the q_e values are equal to $5.16 \text{ mg}\cdot\text{g}^{-1}$ for commercial chitin, $25.13 \text{ mg}\cdot\text{g}^{-1}$ for CS-HW, $20.50 \text{ mg}\cdot\text{g}^{-1}$ for CS-MW and $22.72 \text{ mg}\cdot\text{g}^{-1}$ for CS-LW. At this pH value, the amine groups are protonated to $-\text{NH}_3^+$ and the hydroxyl ones to $-\text{OH}_2^+$. In the case of amide groups, protonation occurs through oxygen [48]. At a pH in the range of 4.0 to 6.0, a significant reduction in the amount of adsorbed Ce(III) ions is observed, which may be due to cerium(III) hydroxide precipitation at higher pH values [49]. On the other hand, the low sorption capacity at low pH 2 may be due to competition of Ce(III) ions with H_3O^+ ions [50]. The significant difference between the sorption properties of commercial chitin and chitosans (Figure 4), may be explained by the higher crystallinity of chitin than chitosan. In turn, crystallinity may affect the availability of reactive functional groups by reducing the level of hydration of the biopolymer molecule [51].

3.2.2. Sorption Time Effect and Kinetic Fitting

Another variable that has a significant impact on the speed of the sorption process is the phase contact time. Figure 6 shows the effect of phase contact time (1–300 min) of Ce(III) ions sorption on eight biopolymers at a concentration of $50 \text{ mg}\cdot\text{L}^{-1}$.

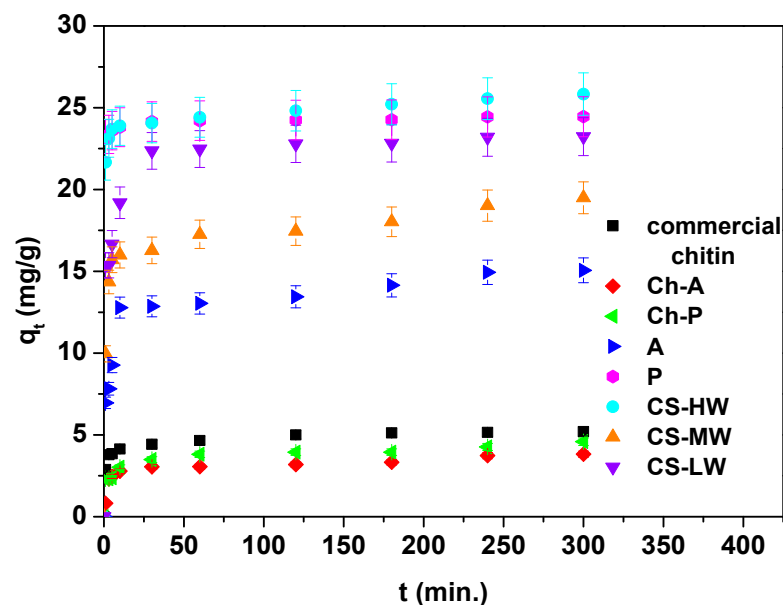


Figure 6. Contact time effect for the Ce(III) ions sorption on commercial chitin, chitin obtained from *H. illucens* adults (Ch-A), chitin derived from *H. illucens* puparia (Ch-P), the ground form of *H. illucens* adults (A), the ground form of *H. illucens* puparia (P), high-molecular-weight commercial chitosan (CS-HW), medium-molecular-weight commercial chitosan (CS-MW), and low-molecular-weight commercial chitosan (CS-LW) (C_0 $50 \text{ mg}\cdot\text{L}^{-1}$, pH 3.0, t 1–300 min., T $25 \text{ }^\circ\text{C}$, 180 rpm).

As can be seen in Figure 6, the kinetic diagram of the adsorption of Ce(III) ions consists of a fast phase at the beginning, where adsorption is rapid before it becomes constant after reaching equilibrium, indicating the exhaustion of access to sorption sites [52,53]. The initial stage's quick adsorption of Ce(III) ions may have been facilitated by the larger concentration gradient and greater availability of free adsorption sites [54]. As is evident from Figure 6, commercial chitin, Ch-A and Ch-P reach equilibrium after 60 min. For A, P and all the chitosan samples, equilibrium is reached after 120–180 min. This is due to the fact that higher amounts of adsorbed Ce(III) ions were obtained for these materials. The q_t values achieved after a time of 300 min are 5.20, 3.82, 4.58, 15.06, 24.45, 25.83, 19.49 and $23.23 \text{ mg}\cdot\text{g}^{-1}$ for commercial chitin, Ch-A and Ch-P, A, P, CS-HW, CS-MW and CS-LW, respectively. In the chitin group, the best results have been attained for commercial chitin, but the q_t values observed for Ch-P are only slightly lower. These are immediately followed

by sample P with a small q_t difference. In general, chitins show significantly lower sorption capacities for Ce(III) ions compared to chitosans. Satisfactory results have been acquired for the ground form of *H. illucens* adults. This last observation should be considered positive because it opens up the possibility of the potential use of *H. illucens* puparia and flies without requiring their conversion into chitin.

Based on a kinetic analysis, the rate and mechanism of the Ce(III) ions adsorption can be assessed. The experimental data have been correlated using three kinetic models in nonlinear forms: the pseudo-first-order (PFO), pseudo-second-order (PSO) and Elovich models. The parameters are listed in Table 2. The nonlinear fitting of kinetic models for Ce(III) ions sorption on biopolymers are presented in Figure S2 (in the Supplementary Materials).

Table 2. Cerium(III) ions sorption parameters for nonlinear kinetic modelling.

Model	Parameters	Sorbent							
		chitin	Ch-A	Ch-P	A	P	CS-HW	CS-MW	CS-LW
	q_e	5.20	3.82	4.58	15.06	24.45	25.83	19.49	23.23
PFO	k_1	0.717	0.310	0.290	0.310	3.232	2.128	0.708	0.853
	q_1	4.70	3.31	3.89	13.75	24.06	24.52	17.40	21.36
	R^2	0.903	0.933	0.782	0.902	0.998	0.987	0.949	0.847
	χ^2	0.222	0.095	0.372	2.038	0.128	0.719	1.580	7.320
PSO	k_2	0.227	0.132	0.133	0.040	0.087	0.240	0.067	0.054
	q_2	4.9	3.47	4.02	14.17	24.19	24.87	18.07	22.42
	R^2	0.966	0.954	0.883	0.950	0.999	0.994	0.978	0.940
	χ^2	0.078	0.065	0.200	1.041	0.498	0.326	0.670	2.871
Elovich	α	1.88×10^3	18.935	55.600	2.84×10^2	7.47×10^{22}	9.73×10^{15}	1.97×10^4	1.93×10^2
	β	2.692	2.536	2.428	0.723	4.321	1.680	0.796	0.628
	R^2	0.992	0.921	0.980	0.960	1.000	0.998	0.965	0.979
	χ^2	0.018	0.112	0.034	0.835	0.079	0.106	1.081	1.010

Non-linear kinetic models: pseudo-first-order (PFO), pseudo-second-order (PSO) and Elovich model. Chitin obtained from *H. illucens* adults (Ch-A), chitin derived from *H. illucens* puparia (Ch-P), the ground form of *H. illucens* adults (A), the ground form of *H. illucens* puparia (P), high-molecular-weight commercial chitosan (CS-HW), medium-molecular-weight commercial chitosan (CS-MW), and low-molecular-weight commercial chitosan (CS-LW).

The PFO model assumes that sorption occurs only at localized sites without interaction with other adsorbed ions. The PSO model, on the other hand, presumes that the amount adsorbed depends not only on time, but also on the concentration of the substance in solution. The third model used to describe the kinetics is the Elovich model. It infers that the activation energy increases as the sorption time increases, and the sorbent surface is considered to be heterogeneous. This model explains the occurrence of adsorption on localized sites and allows for interactions between adsorbed ions [55,56].

To identify the model that best describes the sorption process of Ce(III) ions, the values of determination coefficients and Chi-square errors are compared. The best fit occurs with the Elovich model, for which the highest R^2 values and lowest errors were obtained. The exceptions are the Ch-A and CS-MW samples, for which a better fit is shown by the PSO model. In the case of sorbent W, there is a very good fit with all three kinetic models. This may indicate an interaction of a chemical nature between Ce(III) ions and biopolymers [57].

3.2.3. Effect of Solution Concentration, Isotherm Fitting, and Sorption Comparison

Figure 7 presents the effect in terms of Ce(III) ions sorption of the initial concentration of the solution ($10\text{--}200\text{ mg}\cdot\text{L}^{-1}$) on eight biopolymers at a time of 300 min.

Based on Figure 7, by increasing the initial concentration, the equilibrium capacity of Ce(III) ions increases. With a change in initial concentration from 10 to $200\text{ mg}\cdot\text{L}^{-1}$, the q_e values change as follows: $1.54\text{--}6.98\text{ mg}\cdot\text{g}^{-1}$ for commercial chitin, $1.31\text{--}7.30\text{ mg}\cdot\text{g}^{-1}$ for Ch-A, $1.71\text{--}9.27\text{ mg}\cdot\text{g}^{-1}$ for Ch-P, $5.31\text{--}33.31\text{ mg}\cdot\text{g}^{-1}$ for A, $3.61\text{--}60.96\text{ mg}\cdot\text{g}^{-1}$ for P, $5.32\text{--}37.26\text{ mg}\cdot\text{g}^{-1}$ for CS-HW, $5.13\text{--}26.90\text{ mg}\cdot\text{g}^{-1}$ for CS-MW and $5.13\text{--}33.95\text{ mg}\cdot\text{g}^{-1}$ for CS-LW. This is because the mass transfer is substantially higher, and the beads' active

adsorption sites saturate more quickly. The diffusion of the molecules into the solid is slower for a low starting concentration ($10 \text{ mg}\cdot\text{L}^{-1}$) [58,59]. As in the case of the study of the contact time effect, it is chitin that adsorbs Ce(III) ions with the lowest efficiency. The chitosans and sample A are in second place. For higher concentrations, sample P shows the highest equilibrium capacities. This is an important observation that suggests that samples of only ground fly forms A and P retain their sorption properties in their natural state and do not require additional processing to achieve higher sorption efficiencies.

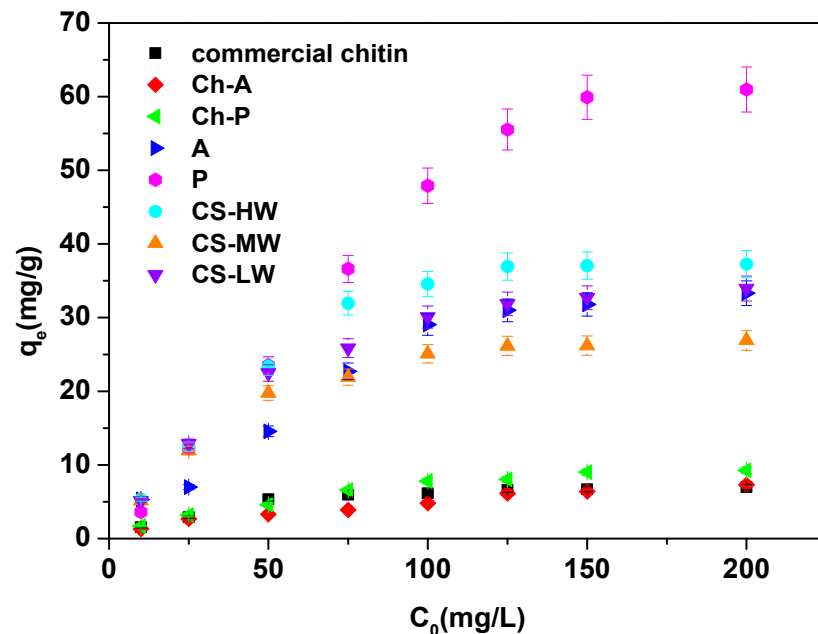


Figure 7. Initial concentration of solution effect for the Ce(III) ions sorption on commercial chitin, chitin obtained from *H. illucens* adults (Ch-A), chitin derived from *H. illucens* puparia (Ch-P), the ground form of *H. illucens* adults (A), the ground form of *H. illucens* puparia (P), high-molecular-weight commercial chitosan (CS-HW), medium-molecular-weight commercial chitosan (CS-MW), and low-molecular-weight commercial chitosan (CS-LW) (C_0 10–200 $\text{mg}\cdot\text{L}^{-1}$, pH 3.0, t 300 min., T 25 °C, 180 rpm).

A total of three sorption isotherms were proposed to describe the Ce(III) ions sorption on biopolymers: the Langmuir, Freundlich and Temkin isotherms in nonlinear forms. The isotherm parameters are summarized in Table 3. The nonlinear fitting of the isotherm models for Ce(III) ions sorption on biopolymers is shown in Figure S3 (in the Supplementary Materials).

The Langmuir isotherm assumes that the adsorbate covers the adsorbent monolayer at specific sorption sites. Additionally, the adsorbate molecules are unable to migrate across the adsorbent's surface and do not interact with one another [60]. On the other hand, the Freundlich model presupposes that there is multilayer adsorption on a heterogeneous surface as opposed to monolayer adsorption on a homogenous material surface [61]. Temkin's model primarily considers the interactions between the adsorbent and adsorbate that take place during the sorption process. Additionally, it assumes that the heat of adsorption of adsorbed molecules linearly decreases as the sorption area's coverage increases [62].

After observing the values of the determination coefficients calculated from the isotherms, the best fit to the Langmuir model can be found. This may indicate a homogeneous and flat adsorption surface, with equally valuable adsorption sites and no interactions between adsorbate molecules at adjacent sites. A good fit, moreover, occurs for the Temkin model. This may suggest some involvement of electrostatic interactions, such as between biopolymer surfaces and Ce(III) ions in the sorption process.

Table 3. Cerium(III) ions sorption parameters for nonlinear isotherm modelling.

Model	Parameters	Sorbent							
		chitin	Ch-A	Ch-P	A	P	CS-HW	CS-MW	CS-LW
Langmuir	q _m	8.08	10.73	12.62	44.93	69.35	37.00	26.48	31.85
	K _L	0.035	0.011	0.017	0.030	0.225	0.804	0.360	0.797
	R ²	0.965	0.948	0.985	0.886	0.959	0.903	0.976	0.916
	χ ²	0.138	0.218	0.115	14.859	20.096	15.040	1.509	9.051
Freundlich	K _F	1.247	0.447	0.865	5.436	20.856	17.554	10.561	13.998
	N	2.947	1.853	2.109	2.531	3.478	5.582	4.866	5.121
	R ²	0.874	0.978	0.953	0.821	0.738	0.834	0.901	0.868
	χ ²	0.494	0.092	0.371	23.326	129.643	25.572	6.199	14.298
Temkin	A	0.398	0.187	0.210	11.640	2.777	47.800	10.572	21.623
	B	1.666	1.890	2.591	4.051	13.305	4.620	3.875	4.404
	R ²	0.942	0.911	0.963	0.697	0.896	0.901	0.971	0.914
	χ ²	0.227	0.377	0.291	52.569	51.667	15.229	1.826	9.179

Chitin obtained from *H. illucens* adults (Ch-A), chitin derived from *H. illucens* puparia (Ch-P), the ground form of *H. illucens* adults (A), the ground form of *H. illucens* puparia (P), high-molecular-weight commercial chitosan (CS-HW), medium-molecular-weight commercial chitosan (CS-MW), and low-molecular-weight commercial chitosan (CS-LW).

In the literature, a growing number of sorbents have been utilized to examine their sorption potential for the removal of cerium(III) ions from aqueous solution (Table 4). Comparing the equilibrium capacities obtained during the study, it can be seen that the results obtained for sample P are comparable to the results obtained using other sorbents. Importantly, this waste does not require processing and is itself a good biosorbent for cerium(III) ions, and its amount is increasing year by year. The use of unmodified waste does not require energy consumption, does not generate additional chemical waste associated with modification, and its use aligns with the principles of a closed-loop economy.

Table 4. Comparison of equilibrium capacities calculated according to the Langmuir model for cerium(III) ions with the literature data.

Sorbent	Equilibrium Capacity (mg·g ⁻¹) According to the Langmuir Model	References
Sodium alginate coated magnetite nanoparticles (Alg-Fe ₃ O ₄)	33.11	[63]
SBA-15 mesoporous silica	27.67	[64]
Clinoptilolite	30.58	[65]
Chitosan-functionalized magnetite-pectin	9.72	[66]
Magnetite (MNP)	76.92	[67]
<i>Pinus brutia</i> leaf powder	17.24	[68]
Magnetic chitosan/yeast	73.53	[69]
Chitin	8.08	This paper
Ch-A	10.73	
Ch-P	12.62	
A	44.93	
P	69.35	
CS-HW	37.00	
CS-MW	26.48	
CS-LW	31.85	

Summarizing our findings, the best adsorption of Ce(III) ions among the investigated samples obtained from *H. illucens* and the commercial materials occurred at pH 3. At a starting concentration of 50 mg Ce·L⁻¹, all the chitins reached equilibrium faster (60 min) than the raw materials and chitosans (120–180 min). Under these conditions and after

300 min, the highest adsorption properties were expressed by high-molecular-weight commercial chitosan ($25.83 \text{ mg}\cdot\text{g}^{-1}$), although the ground form of *H. illucens* puparia ($24.45 \text{ mg}\cdot\text{g}^{-1}$) was very close to this level. The second raw material, the ground form of *H. illucens* adults ($15.06 \text{ mg}\cdot\text{g}^{-1}$), was placed in an intermediate position between high-molecular-weight commercial chitosan and chitins. The weakest adsorption properties were shown by chitins and the difference between commercial ones and those from *H. illucens* was minimal ($5.20 \text{ mg}\cdot\text{g}^{-1}$ commercial vs. $3.82 \text{ mg}\cdot\text{g}^{-1}$ for chitin obtained from *H. illucens* adult flies and $4.58 \text{ mg}\cdot\text{g}^{-1}$ for chitin derived from *H. illucens* puparia).

The effect of the initial Ce(III) concentration on its adsorption measured after 300 min was not considerable for all the chitins studied (the max q_e values for the commercial chitin, chitin obtained from *H. illucens* adults flies, and chitin derived from *H. illucens* puparia were 6.98, 7.30, and $9.27 \text{ mg}\cdot\text{g}^{-1}$, respectively). The most interesting finding was that the material with the highest adsorption capacity was the ground form of *H. illucens* puparia ($60.96 \text{ mg}\cdot\text{g}^{-1}$), while the ground form of *H. illucens* adults ($33.31 \text{ mg}\cdot\text{g}^{-1}$) was placed at a level similar to all the commercial chitosans tested (37.26 , 26.90 , and $33.95 \text{ mg}\cdot\text{g}^{-1}$ for high-molecular-weight commercial chitosan, medium-molecular-weight commercial chitosan, and low-molecular-weight commercial chitosan—CS-LW, respectively). All the tested materials under these conditions had the best fit to the Langmuir model, with the exception of chitin obtained from *H. illucens* adults flies, where the best fit occurred for the Freundlich model.

4. Conclusions

The results of this research clearly showed that wastes from *H. illucens* breeding in the form of puparia and dead adults did not require processing and were themselves good biosorbents for cerium. Untreated chitinous waste had significantly better sorption properties for Ce(III) than the purified chitin extracted from them. However, chitins from *H. illucens* had slightly better adsorption properties than commercial marine chitin, but the difference was low. The use of unmodified waste does not require any energy inputs and does not cause additional chemical waste after chemical modification. Due to increase in insect breeding worldwide, the amount of this type of waste will be also increasing. Thus, the use of this waste fits particularly well with the principles of the circular economy. In the future, on the basis of our findings, testing the ability for absorption of other ions should be checked. This study provides a good justification for the broad testing of puparia and dead adults as biosorbents for real wastewater.

Supplementary Materials: The following supporting information can be downloaded at: <https://www.mdpi.com/article/10.3390/ma17215255/s1>, Figure S1: EDS patterns for (a) commercial chitin, (b) CS-HW, (c) CS-MW, (d) CS-LW; Figure S2: Nonlinear fitting of kinetic models for the Ce(III) ions sorption on (a) commercial chitin, (b) Ch-I, (c) Ch-W (d) I, (e) W, (f) CS-HW, (g) CS-MW, (h) CS-LW; Figure S3: Nonlinear fitting of isotherm models for the Ce(III) ions sorption on (a) commercial chitin, (b) Ch-I, (c) Ch-W (d) I, (e) W, (f) CS-HW, (g) CS-MW, (h) CS-LW; Table S1: Circle Equivalent (CE) diameter distribution of tested materials presented in percentiles sections. CE diameter is the diameter of a circle with the same area as the 2D image of the particle.

Author Contributions: Conceptualization, J.B. and P.B.; methodology, J.B., P.B., D.K. and A.B.; formal analysis, J.B., P.B. and M.K.; investigation, J.B., P.B. and M.K.; data curation, J.B., P.B. and M.K.; writing—original draft preparation, J.B., P.B. and M.K.; writing—review and editing, J.B., P.B., M.K., D.K. and A.B.; visualization, J.B.; supervision, D.K. and A.B.; project administration, P.B.; funding acquisition, P.B. All authors have read and agreed to the published version of the manuscript.

Funding: This work was partially funded by the National Science Centre, Poland, Grant Number 2019/35/D/NZ9/01835. Funding source had no influence on study design, collection and data analysis, data interpretation, writing the manuscript nor the decision to submit the article for publication. The APC have been granted by MDPI.

Institutional Review Board Statement: Not applicable.

Informed Consent Statement: This study used the empty pupae shells (puparia) of the insect *Hermetia illucens*. Live insects have not been the object of study in any of their developmental forms. Puparia are left by emerging pupae naturally, and their gathering does not require the killing of the insect.

Data Availability Statement: Data may be provided upon request to the corresponding author.

Conflicts of Interest: The funders had no role in the design of the study; in the collection, analyses, or interpretation of data; in the writing of the manuscript; or in the decision to publish the results.

References

1. Jowitt, S.M.; Werner, T.T.; Weng, Z.; Mudd, G.M. Recycling of the Rare Earth Elements. *Curr. Opin. Green Sustain. Chem.* **2018**, *13*, 1–7. [[CrossRef](#)]
2. Saviano, L.; Brouziotis, A.A.; Suarez, E.G.P.; Siciliano, A.; Spampinato, M.; Guida, M.; Trifuoggi, M.; Del Bianco, D.; Carotenuto, M.; Spica, V.R.; et al. Catalytic Activity of Rare Earth Elements (REEs) in Advanced Oxidation Processes of Wastewater Pollutants: A Review. *Molecules* **2023**, *28*, 6185. [[CrossRef](#)] [[PubMed](#)]
3. Bessais, L. Structure and Magnetic Properties of Intermetallic Rare-Earth-Transition-Metal Compounds: A Review. *Materials* **2022**, *15*, 201. [[CrossRef](#)] [[PubMed](#)]
4. Song, X.; Chang, M.H.; Pecht, M. Rare-Earth Elements in Lighting and Optical Applications and Their Recycling. *JOM* **2013**, *65*, 1276–1282. [[CrossRef](#)]
5. Balaram, V. Rare Earth Elements: A Review of Applications, Occurrence, Exploration, Analysis, Recycling, and Environmental Impact. *Geosci. Front.* **2019**, *10*, 1285–1303. [[CrossRef](#)]
6. Weng, Z.; Jowitt, S.M.; Mudd, G.M.; Haque, N. A Detailed Assessment of Global Rare Earth Element Resources: Opportunities and Challenges. *Econ. Geol.* **2015**, *110*, 1925–1952. [[CrossRef](#)]
7. Kilbourn, B.T. Cerium and Cerium Compounds. In *Kirk-Othmer Encyclopedia of Chemical Technology*; Wiley: Hoboken, NJ, USA, 2011; Volume 5, pp. 670–692.
8. Barker, E.; Shepherd, J.; Asencio, I.O. The Use of Cerium Compounds as Antimicrobials for Biomedical Applications. *Molecules* **2022**, *27*, 2678. [[CrossRef](#)]
9. Dahle, J.T.; Arai, Y. Environmental Geochemistry of Cerium: Applications and Toxicology of Cerium Oxide Nanoparticles. *Int. J. Environ. Res. Public Health* **2015**, *12*, 1253–1278. [[CrossRef](#)]
10. Hamza, M.F.; Guibal, E.; Abdel-rahman, A.A.; Salem, M.; Khalafalla, M.S.; Wei, Y.; Yin, X. Magnetite Chitosan Microparticles by Sorbent Sulfonation—Application to Ore Leachate. *Molecules* **2022**, *27*, 7562. [[CrossRef](#)]
11. Lo, Y.C.; Cheng, C.L.; Han, Y.L.; Chen, B.Y.; Chang, J.S. Recovery of High-Value Metals from Geothermal Sites by Biosorption and Bioaccumulation. *Bioresour. Technol.* **2014**, *160*, 182–190. [[CrossRef](#)]
12. Hsu, S.T.; Lin, W.C.; Hsiao, W.F.; Lee, C.C.; Pan, T.C.; Wang, T.T.; Huang, Y.M. Preparation of Methacrylic Acid-Grafted Chitin Using Cerium (IV) Ion and Its Application in Adsorbing Paraquat. *J. Appl. Polym. Sci.* **2013**, *127*, 760–764. [[CrossRef](#)]
13. Abd El-Magied, M.O. High-Efficiency Recovery of Cerium Ions from Monazite Leach Liquor by Polyamines and Polycarboxylates Chitosan Sorbents Prepared from Marine Industrial Wastes. *Int. J. Biol. Macromol.* **2023**, *243*, 125243. [[CrossRef](#)] [[PubMed](#)]
14. Aljohani, M.S.; Alnoman, R.B.; Alharbi, H.Y.; Bukhari, A.A.H.; Monier, M. Development and Evaluation of Thiosalicylic-Modified/Ion-Imprinted Chitosan for Selective Removal of Cerium (III) Ion. *Carbohydr. Polym.* **2024**, *326*, 121620. [[CrossRef](#)] [[PubMed](#)]
15. Kano, N.; Pang, M.; Deng, Y.; Imaizumi, H. Adsorption of Rare Earth Elements (REEs) onto Activated Carbon Modified with Potassium Permanganate (KMnO₄). *J. Appl. Solut. Chem. Model.* **2017**, *6*, 51–61. [[CrossRef](#)]
16. Sert, Ş.; Kütahyalı, C.; Inan, S.; Talip, Z.; Çetinkaya, B.; Eral, M. Biosorption of Lanthanum and Cerium from Aqueous Solutions by *Platanus Orientalis* Leaf Powder. *Hydrometallurgy* **2008**, *90*, 13–18. [[CrossRef](#)]
17. Sadovsky, D.; Brenner, A.; Astrachan, B.; Asaf, B.; Gonen, R. Biosorption Potential of Cerium Ions Using *Spirulina* Biomass. *J. Rare Earths* **2016**, *34*, 644–652. [[CrossRef](#)]
18. Vijayaraghavan, K.; Sathishkumar, M.; Balasubramanian, R. Biosorption of Lanthanum, Cerium, Europium, and Ytterbium by a Brown Marine Alga, *Turbinaria Conoides*. *Ind. Eng. Chem. Res.* **2010**, *49*, 4405–4411. [[CrossRef](#)]
19. Vijayaraghavan, K.; Balasubramanian, R. Single and Binary Biosorption of Cerium and Europium onto Crab Shell Particles. *Chem. Eng. J.* **2010**, *163*, 337–343. [[CrossRef](#)]
20. Barragan-Fonseca, K.B.; Dicke, M.; van Loon, J.J.A. Nutritional Value of the Black Soldier Fly (*Hermetia illucens* L.) and Its Suitability as Animal Feed—A Review. *J. Insects Food Feed* **2017**, *3*, 105–120. [[CrossRef](#)]
21. Barrett, M.; Chia, S.Y.; Fischer, B.; Tomberlin, J.K. Welfare Considerations for Farming Black Soldier Flies, *Hermetia illucens* (Diptera: Stratiomyidae): A Model for the Insects as Food and Feed Industry. *J. Insects Food Feed* **2023**, *9*, 119–148. [[CrossRef](#)]
22. Guarnieri, A.; Triunfo, M.; Scieuzo, C.; Ianniciello, D.; Tafi, E.; Hahn, T.; Zibek, S.; Salvia, R.; De Bonis, A.; Falabella, P. Antimicrobial Properties of Chitosan from Different Developmental Stages of the Bioconverter Insect *Hermetia illucens*. *Sci. Rep.* **2022**, *12*, 8084. [[CrossRef](#)] [[PubMed](#)]
23. Bulak, P.; Proc-Pietrycha, K.; Kaczor, M.; Złotko, K.; Polakowski, C.; Wiącek, D.; Waniak-Nowicka, H.; Zięba, E.; Waśko, A.; Oleszczuk, P.; et al. A Novel Type of Biochar from Chitinous *Hermetia illucens* Waste with a Built-in Stimulating Effect on Plants and Soil Arthropods. *Sci. Rep.* **2023**, *13*, 8306. [[CrossRef](#)] [[PubMed](#)]

24. Purkayastha, D.; Sarkar, S. Physicochemical Structure Analysis of Chitin Extracted from Pupa Exuviae and Dead Imago of Wild Black Soldier Fly (*Hermetia illucens*). *J. Polym. Environ.* **2020**, *28*, 445–457. [\[CrossRef\]](#)
25. Proc, K.; Bulak, P.; Wiącek, D.; Bieganowski, A. *Hermetia illucens* Exhibits Bioaccumulative Potential for 15 Different Elements—Implications for Feed and Food Production. *Sci. Total Environ.* **2020**, *723*, 138125. [\[CrossRef\]](#)
26. Złotko, K.; Waśko, A.; Kamiński, D.M.; Budziak-Wieczorek, I.; Bulak, P.; Bieganowski, A. Isolation of Chitin from Black Soldier Fly (*Hermetia illucens*) and Its Usage to Metal Sorption. *Polymers* **2021**, *13*, 818. [\[CrossRef\]](#)
27. Gharibzadeh, M.; Osfouri, S.; Jamekhorshid, A.; Jafari, S.A. Microbial Chitin Extraction and Characterization from Green Tiger Shrimp Waste: A Comparative Study of Culture Mediums along with Bioprocess Optimization. *Int. J. Biol. Macromol.* **2023**, *242*, 125213. [\[CrossRef\]](#)
28. Liu, Y.; Liu, R.; Shi, J.; Zhang, R.; Tang, H.; Xie, C.; Wang, F.; Han, J.; Jiang, L. Chitosan/Esterified Chitin Nanofibers Nanocomposite Films Incorporated with Rose Essential Oil: Structure, Physicochemical Characterization, Antioxidant and Antibacterial Properties. *Food Chem. X* **2023**, *18*, 100714. [\[CrossRef\]](#)
29. Waśko, A.; Bulak, P.; Polak-Berecka, M.; Nowak, K.; Polakowski, C.; Bieganowski, A. The First Report of the Physicochemical Structure of Chitin Isolated from *Hermetia illucens*. *Int. J. Biol. Macromol.* **2016**, *92*, 316–320. [\[CrossRef\]](#)
30. Jampafuang, Y.; Tongta, A.; Waiprib, Y. Impact of Crystalline Structural Differences between α - and β -Chitosan on Their Nanoparticle Formation. *Polymers* **2019**, *11*, 2010. [\[CrossRef\]](#)
31. Jena, K.; Ananta, S.; Akthar, J.; Patnaik, A.; Das, S.; Singh, J.; Sathyanarayana, K.; Kar, P.K.; Das, B.K.; Hassan, M.A.; et al. Physical, Biochemical and Antimicrobial Characterization of Chitosan Prepared from Tasar Silkworm Pupae Waste. *Environ. Technol. Innov.* **2023**, *31*, 103200. [\[CrossRef\]](#)
32. Alimi, B.A.; Hoque, M.; Pathania, S.; Wilson, J.; Duffy, B.; Celayeta Frias, J.M. Structural, Thermal, Optical, and Mechanical Properties of Composite Films Developed from the Button Mushroom (*Agaricus bisporus*)-Sourced High Molecular Weight Chitosan and Potato Starch. *LWT Food Sci. Technol.* **2023**, *185*, 115201. [\[CrossRef\]](#)
33. Jyoti; Singh, S.; Das, S.; Srivastava, S. Comparative Study for Removal of Toxic Hexavalent Chromium by Zinc Oxide Nanoparticles, Chitosan, Chitin and Zinc-Chitosan Nano-Biocomposite. *Environ. Technol. Innov.* **2023**, *32*, 103310. [\[CrossRef\]](#)
34. Zhuikova, Y.V.; Zhuikov, V.A.; Makhina, T.K.; Efremov, Y.M.; Aksenova, N.A.; Timashev, P.S.; Bonartseva, G.A.; Varlamov, V.P. Preparation and Characterization of Poly(3-Hydroxybutyrate)/Chitosan Composite Films Using Acetic Acid as a Solvent. *Int. J. Biol. Macromol.* **2023**, *248*, 125970. [\[CrossRef\]](#) [\[PubMed\]](#)
35. Hamdan, Y.A.; Elouali, S.; Eladlani, N.; Lefeuvre, B.; Oudadesse, H.; Rhazi, M. Investigation on *Akis granulifera* (Coleoptera, Sahlberg, 1823) as a Potential Source of Chitin and Chitosan: Extraction, Characterization and Hydrogel Formation. *Int. J. Biol. Macromol.* **2023**, *252*, 126292. [\[CrossRef\]](#)
36. Zhu, H.; Tang, H.; Li, F.; Sun, H.; Tong, L. Effect of Milling Intensity on the Properties of Chitin, Chitosan and Chitosan Films Obtained from Grasshopper. *Int. J. Biol. Macromol.* **2023**, *239*, 124249. [\[CrossRef\]](#)
37. Dotto, G.L.; Pinto, L.A.A. Adsorption of Food Dyes onto Chitosan: Optimization Process and Kinetic. *Carbohydr. Polym.* **2011**, *84*, 231–238. [\[CrossRef\]](#)
38. Franco, D.S.P.; Vieillard, J.; Salau, N.P.G.; Dotto, G.L. Interpretations on the Mechanism of In(III) Adsorption onto Chitosan and Chitin: A Mass Transfer Model Approach. *J. Mol. Liq.* **2020**, *304*, 112758. [\[CrossRef\]](#)
39. Shinu, K.P.; John, H.; Gopalakrishnan, J. Chitin/Deacetylated Chitin Nanocomposite Film for Effective Adsorption of Organic Pollutant from Aqueous Solution. *Int. J. Biol. Macromol.* **2023**, *242*, 125038. [\[CrossRef\]](#)
40. Rahman, T.U.; Roy, H.; Shoronika, A.Z.; Fariha, A.; Hasan, M.; Islam, M.S.; Marwani, H.M.; Islam, A.; Hasan, M.M.; Alsukaibi, A.K.D.; et al. Sustainable Toxic Dye Removal and Degradation from Wastewater Using Novel Chitosan-Modified TiO₂ and ZnO Nanocomposites. *J. Mol. Liq.* **2023**, *388*, 122764. [\[CrossRef\]](#)
41. Rakshit, S.; Pal, K.; Mondal, S.; Jana, A.; Mondal, K.C.; Halder, S.K. Extraction of Chitosan from Biologically-Derived Chitin by Bacterial Chitin Deacetylase: Process Optimization and Product Quality Assessment. *Int. J. Biol. Macromol.* **2023**, *244*, 125389. [\[CrossRef\]](#)
42. Bhavsar, P.S.; Dalla Fontana, G.; Zoccola, M. Sustainable Superheated Water Hydrolysis of Black Soldier Fly Exuviae for Chitin Extraction and Use of the Obtained Chitosan in the Textile Field. *ACS Omega* **2021**, *6*, 8884–8893. [\[CrossRef\]](#) [\[PubMed\]](#)
43. Boykin, K.L.; Carter, R.T.; Butler-Perez, K.; Buck, C.Q.; Peters, J.W.; Rockwell, K.E.; Mitchell, M.A. Digestibility of Black Soldier Fly Larvae (*Hermetia illucens*) Fed to Leopard Geckos (*Eublepharis macularius*). *PLoS ONE* **2020**, *15*, e0232496. [\[CrossRef\]](#) [\[PubMed\]](#)
44. Kaczor, M.; Bulak, P.; Proc-Pietrycha, K.; Kirichenko-Babko, M.; Bieganowski, A. The Variety of Applications of *Hermetia illucens* in Industrial and Agricultural Areas—Review. *Biology* **2023**, *12*, 25. [\[CrossRef\]](#) [\[PubMed\]](#)
45. Hahn, T.; Tafi, E.; von Seggern, N.; Falabella, P.; Salvia, R.; Thomä, J.; Febel, E.; Fijalkowska, M.; Schmitt, E.; Stegbauer, L.; et al. Purification of Chitin from Pupal Exuviae of the Black Soldier Fly. *Waste Biomass Valorization* **2022**, *13*, 1993–2008. [\[CrossRef\]](#)
46. Triunfo, M.; Tafi, E.; Guarnieri, A.; Salvia, R.; Scieuzo, C.; Hahn, T.; Zibek, S.; Gagliardini, A.; Panariello, L.; Coltelli, M.B.; et al. Characterization of Chitin and Chitosan Derived from *Hermetia illucens*, a Further Step in a Circular Economy Process. *Sci. Rep.* **2022**, *12*, 6613. [\[CrossRef\]](#)
47. Zhou, P.; Li, J.; Yan, T.; Wang, X.; Huang, J.; Kuang, Z.; Ye, M.; Pan, M. Selectivity of Deproteinization and Demineralization Using Natural Deep Eutectic Solvents for Production of Insect Chitin (*Hermetia illucens*). *Carbohydr. Polym.* **2019**, *225*, 115255. [\[CrossRef\]](#)

48. El Harmoudi, H.; El Gaini, L.; Daoudi, E.; Rhazi, M.; Boughaleb, Y.; El Mhammedi, M.A.; Migalska-Zalas, A.; Bakasse, M. Removal of 2,4-D from Aqueous Solutions by Adsorption Processes Using Two Biopolymers: Chitin and Chitosan and Their Optical Properties. *Opt. Mater.* **2014**, *36*, 1471–1477. [[CrossRef](#)]
49. Kołodzyńska, D.; Bąk, J.; Majdańska, M.; Fila, D. Sorption of Lanthanide Ions on Biochar Composites. *J. Rare Earths* **2018**, *36*, 1212–1220. [[CrossRef](#)]
50. Hanafiah, M.A.K.M.; Ariff, N.F.M.; Ibrahim, S.; Ngah, W.S.W.; Hussain, Z.M. Synthesis of Xanthated Chitosan Beads for Fast and Efficient Recovery of Precious Ce(III) Ions from Aqueous Solutions. *Desalin. Water Treat.* **2020**, *204*, 257–269. [[CrossRef](#)]
51. Guibal, E.; Vincent, T.; Navarro, R. Metal Ion Biosorption on Chitosan for the Synthesis of Advanced Materials. *J. Mater. Sci.* **2014**, *49*, 5505–5518. [[CrossRef](#)]
52. Thabede, P.M.; Khumalo, N.A.H.; Mahlambi, P.N.; Nyamukamba, P.; Modise, S.J. Sorption of Ibuprofen by Chemically Treated Maize Cob. *South Afr. J. Chem. Eng.* **2023**, *46*, 376–385. [[CrossRef](#)]
53. Hafshejani, L.D.; Nasab, S.B.; Gholami, R.M.; Moradzadeh, M.; Izadpanah, Z.; Hafshejani, S.B.; Bhatnagar, A. Removal of Zinc and Lead from Aqueous Solution by Nanostructured Cedar Leaf Ash as Biosorbent. *J. Mol. Liq.* **2015**, *211*, 448–456. [[CrossRef](#)]
54. Nekhunguni, P.M.; Tavengwa, N.T.; Tutu, H. Sorption of Uranium(VI) onto Hydrous Ferric Oxide-Modified Zeolite: Assessment of the Effect of pH, Contact Time, Temperature, Selected Cations and Anions on Sorbent Interactions. *J. Environ. Manag.* **2017**, *204*, 571–582. [[CrossRef](#)] [[PubMed](#)]
55. Largette, L.; Pasquier, R. A Review of the Kinetics Adsorption Models and Their Application to the Adsorption of Lead by an Activated Carbon. *Chem. Eng. Res. Des.* **2016**, *109*, 495–504. [[CrossRef](#)]
56. Lima, J.Z.; Ferreira da Silva, E.; Patinha, C.; Durães, N.; Vieira, E.M.; Rodrigues, V.G.S. Sorption of Arsenic by Composts and Biochars Derived from the Organic Fraction of Municipal Solid Wastes: Kinetic, Isotherm and Oral Bioaccessibility Study. *Environ. Res.* **2022**, *204*, 111988. [[CrossRef](#)]
57. Bąk, J.; Gustaw, S.; Kołodzyńska, D. The Use of Eggshells, Boiler Stone, Chalk and Marl for the Synthesis of Novel Hydroxyapatite Modified Biochars for the Vanadium Removal. *Chem. Eng. J.* **2023**, *470*, 144309. [[CrossRef](#)]
58. Novais, R.M.; Carvalheiras, J.; Tobaldi, D.M.; Seabra, M.P.; Pullar, R.C.; Labrincha, J.A. Synthesis of Porous Biomass Fly Ash-Based Geopolymer Spheres for Efficient Removal of Methylene Blue from Wastewaters. *J. Clean. Prod.* **2019**, *207*, 350–362. [[CrossRef](#)]
59. Aichour, A.; Zaghouane-Boudiaf, H.; Mohamed Zuki, F.B.; Kheireddine Aroua, M.; Ibbora, C.V. Low-Cost, Biodegradable and Highly Effective Adsorbents for Batch and Column Fixed Bed Adsorption Processes of Methylene Blue. *J. Environ. Chem. Eng.* **2019**, *7*, 103409. [[CrossRef](#)]
60. Jaworska, M.M.; Filipkowska, U.; Modrzejewska, Z. Adsorption of the Dye Acid Blue 158 Premetalized with Chromium on Chitin/Chitosan. *Carbohydr. Polym.* **2022**, *298*, 120122. [[CrossRef](#)]
61. Wang, L.; Li, Z.; Wang, Y.; Brookes, P.C.; Wang, F.; Zhang, Q.; Xu, J.; Liu, X. Performance and Mechanisms for Remediation of Cd(II) and As(III) Co-Contamination by Magnetic Biochar-Microbe Biochemical Composite: Competition and Synergy Effects. *Sci. Total Environ.* **2021**, *750*, 141672. [[CrossRef](#)]
62. Maamoun, I.; Eljamal, R.; Falyouna, O.; Bensaida, K.; Sugihara, Y.; Eljamal, O. Insights into Kinetics, Isotherms and Thermodynamics of Phosphorus Sorption onto Nanoscale Zero-Valent Iron. *J. Mol. Liq.* **2021**, *328*, 115402. [[CrossRef](#)]
63. Serunting, M.A.; Rusnadi, R.; Setyorini, D.A.; Ramadan, B.S. An Effective Cerium (III) Ions Removal Method Using Sodium Alginate-Coated Magnetite (Alg-Fe₃O₄) Nanoparticles. *J. Water Supply Res. Technol. AQUA* **2018**, *67*, 754–765. [[CrossRef](#)]
64. Zare-Dorabei, R.; Jalalat, V.; Tadjarodi, A. Central Composite Design Optimization of Ce(III) Ion Removal from Aqueous Solution Using Modified SBA-15 Mesoporous Silica. *New J. Chem.* **2016**, *40*, 5128–5134. [[CrossRef](#)]
65. Fila, D.; Hubicki, Z.; Kołodzyńska, D. Applicability of New Sustainable and Efficient Alginate-Based Composites for Critical Raw Materials Recovery: General Composites Fabrication Optimization and Adsorption Performance Evaluation. *Chem. Eng. J.* **2022**, *446*, 137245. [[CrossRef](#)]
66. Chaibou Yacouba, A.-R.; Oral, A.E.; Sert, S.; Kaptanoglu, I.G.; Natatou, I.; Yusan, S.; Aytas, S. Removal of Lanthanum and Cerium from Aqueous Solution Using Chitosan-Functionalized Magnetite-Pectin. *Discov. Water* **2024**, *4*, 1. [[CrossRef](#)]
67. Akbas, Y.A.; Yusan, S.; Sert, S.; Aytas, S. Sorption of Ce(III) on Magnetic/Olive Pomace Nanocomposite: Isotherm, Kinetic and Thermodynamic Studies. *Environ. Sci. Pollut. Res.* **2021**, *28*, 56782–56794. [[CrossRef](#)]
68. Kütahyalı, C.; Şert, S.; Çetinkaya, B.; Inan, S.; Eral, M. Factors Affecting Lanthanum and Cerium Biosorption on *Pinus brutia* Leaf Powder. *Sep. Sci. Technol.* **2010**, *45*, 1456–1462. [[CrossRef](#)]
69. Ou, H.X.; Bian, W.B.; Weng, X.M.; Huang, W.H.; Zhang, Y.L. Adsorption of Ce(III) by Magnetic Chitosan/Yeast Composites from Aqueous Solution: Kinetic and Equilibrium Studies. *Appl. Mech. Mater.* **2013**, *316–317*, 391–394. [[CrossRef](#)]

Disclaimer/Publisher's Note: The statements, opinions and data contained in all publications are solely those of the individual author(s) and contributor(s) and not of MDPI and/or the editor(s). MDPI and/or the editor(s) disclaim responsibility for any injury to people or property resulting from any ideas, methods, instructions or products referred to in the content.